Reconstructing images in electrical impedance tomography using hybrid genetic algorithms

Renier G. Mendoza[1] and Jose Ernie C. Lope[2]
Institute of Mathematics, College of Science
University of the Philippines Diliman, C.P. Garcia Avenue, Diliman 1101 Quezon City, Philippines
(632) 928-0439 [1] Email: mendoza.renier@gmail.com; [2] Email: ernie@math.upd.edu.ph

ABSTRACT

In electrical impedance tomography (EIT), current patterns I_l $(l = 1,2,\ldots,L)$ are injected to a body through L electrodes and the corresponding voltages V_l $(l = 1,2,\ldots,L)$ are then measured. Based on these measurements, image reconstruction is done by solving an inverse problem involving the generalized Laplace equation $-\nabla \cdot (\sigma \nabla \phi) = 0$ on Ω, where σ is the conductivity distribution and ϕ is the electric potential over Ω. Using the known quantities I_l and V_l, we wish to recover the geometry and conductivity σ within the body.

In this work, we considered the case where the body Ω is a unit square and has two square-shaped cavities with constant conductivities. The forward problem was solved using the finite element method while the inverse problem was posed as a minimization problem. We then explored the use of the genetic algorithm (GA) hybridized with another heuristic algorithm (simulated annealing) and two deterministic algorithms (Nelder-Mead simplex method and Quasi-Newton method) in solving the optimization problem. Our numerical simulations showed that the proposed hybrids of the GA could best recover the conductivity distribution if the geometry inside the body was known.

Keywords: Electrical impedance, tomography, hybrid genetic and algorithms

INTRODUCTION

Electrical Impedance Tomography (EIT) is an imaging technique that tries to recover the spatial distribution of the conductivities in the interior of a body Ω based on electrical measurements from electrodes placed around its boundary $\partial\Omega$. The measured voltage drops are due to known current patterns that are injected through the same electrodes. This non-invasive technique has a wide range of applications, from breast cancer detection (Cheney and others 1999) to locating underground mineral deposits (Parker 1984) and the detection of corrosion in metals (Santosa and others 1996).

Let us assume that the body Ω has cavities at unknown locations in its interior. If the conductivities on these cavities show good contrast with the surrounding region, then the imaging of Ω can be done using EIT.For example, the specific conductance (conductivity) of human tissues varies from 15.4 mS/cm for the cerebrospinal fluid to 0.06 mS/cm for the bone. This means that the cross-sectional images of the conductivity distribution inside the human body should show good contrast, and thus EIT can be applied.

The problem of image reconstruction via EIT consists of two sub-problems: the forward problem and the inverse problem. In the forward EIT problem, we solve for the boundary voltages given the conductivity distribution σ over Ω and the currents at the boundary. This is done by solving a generalized Laplace equation subject to some boundary conditions. The boundary currents are chosen in such a way that the law of conservation of charge is preserved. On the other hand, the inverse EIT problem, also known as the image reconstruction problem, is the recovery of the conductivity distribution inside Ω given the voltage and current measurements at the boundary. A satisfactory solution, though, is difficult to obtain because the EIT problem is ill-posed (Borcea 2006), i.e., small changes in the boundary data could result in large changes in the conductivity distribution of the interior of Ω.

In this paper, we used the finite element method (FEM) to solve the forward problem. As for the inverse problem, we posed it as an optimization problem and iteratively searched for an estimate of the conductivity distribution σ over Ω that corresponds to the measured boundary voltages and currents. While the paper by Kim H-C and others (2005) obtained good results, they only considered the case of finding the conductivity of the body when the geometry is known. On the other hand, da Silva Barra and others (2006) solved the inverse EIT problem also with GA but they only did a geometric reconstruction. Moreover, our method obtained a lower residual value. Our numerical simulations showed that hybrids of the GA could more effectively solve the optimization problem, thereby allowing a more accurate recovery of the locations of the cavities or the values of the conductivities inside Ω, or both quantities if both are unknown.

MATHEMATICAL FOUNDATION

Consider a body Ω with boundary $\partial\Omega$ and conductivity distribution σ. The simplest reconstruction model, known as the Continuum Model of the EIT Problem, states that if the normal current density is prescribed on $\partial\Omega$, then the distribution of the electric potential ϕ on the whole body is uniquely determined.

Theorem 1 (Continuum model)

Suppose $\Omega \subset \mathbb{R}^n$ is a bounded and connected domain with sufficiently smooth boundary $\partial\Omega$, conductivity $\sigma \in L^\infty(\Omega)$ and that a flux $f \in L^2(\partial\Omega)$, with $\int_{\partial\Omega} f dS = 0$, is applied on $\partial\Omega$. Then the corresponding induced electrical potential $\phi \in H^1(\Omega)$ can be uniquely determined through the partial differential equation,

$$-\nabla \cdot (\sigma \nabla \phi) = 0 \quad on \ \Omega, \tag{1}$$

subject to the boundary condition,

$$\sigma \frac{\partial \phi}{\partial n} = f \text{ on } \partial\Omega. \tag{2}$$

This can be proved using standard argument: we multiply (1) by $v \in H^1(\Omega)$ and use the Divergence theorem and Equation (2) to obtain the variational formulation. It is then easily shown that the Lax-Milgram theorem applies, and thus we obtain a unique weak solution in $H^1(\Omega)$.

However, this model of EIT does not apply in reality because we only know partial information on the

boundary, i.e., electrical currents are injected through the L electrodes and not on the whole of $\partial\Omega$. Thus, there is a need to modify the boundary condition (2). Let $e_l \subset \partial\Omega$ be an electrode attached to the boundary. Suppose electrical currents I_l ($l = 1,2,...,L$) are injected into the body Ω through these electrodes e_l ($l = 1,2,...,L$) attached on the boundary $\partial\Omega$, and let $\Gamma = \bigcup_{l=1}^{L} e_l$ and $\Gamma' = \partial\Omega - \Gamma$. Moreover, let V_l be the measured voltage at the lth electrode. We pose the following new boundary conditions:

$$\int_{e_l} \sigma \frac{\partial \phi}{\partial n} dS = I_l \quad \text{for } 1 \le l \le L, \tag{3}$$

$$\sigma \frac{\partial \phi}{\partial n} = 0 \quad \text{on } \Gamma', \tag{4}$$

$$\phi + z_l \sigma \frac{\partial \phi}{\partial n} = V_l \quad \text{on } \Gamma. \tag{5}$$

Condition (3) simply means that the integral of the current density over the electrode is equal to the total current that flows to that electrode. Condition (4) means that no current flows in the gaps between the electrodes. Finally, condition (5) means that the voltage under each electrode is not constant but rather drops across the contact impedance layer (e.g., the human skin) with impedance z_l. The impedance can vary over e_l but shall be assumed constant for simplicity.

These new boundary conditions together with Eq. (1) give us the *Complete Electrode Model*, which is the EIT model used in this study. In addition to the boundary conditions, we have the following standard conditions for the injected current and measured voltages by considering the conservation of the electric charge and appropriate selection of the electrodes:

$$\sum_{i=1}^{L} I_l \quad \text{and} \quad \sum_{i=1}^{L} V_l = 0. \tag{6}$$

The Complete Electrode Model is also known to have a unique solution $\phi \in H^1(\Omega)$. In fact, a whole section in the article of Somersalo and others (1992) is dedicated to the existence and uniqueness of the solution of this model.

Solving the forward problem

We considered the simple case where Ω is the rectangular region $[0,1] \times [0,1]$ and that the conductivity σ is piecewise constant over Ω, i.e.,

$$\sigma = \begin{cases} \sigma_1, & (x,y) \in \Omega_a, \\ \sigma_2, & (x,y) \in \Omega_b, \\ \sigma_3, & \text{elsewhere}, \end{cases} \tag{7}$$

where Ω_a and Ω_b are disjoint, rectangular subregions of Ω. We took the values σ_i's from Table 1, which lists the actual conductivities of the human blood and internal organs (Gray 2002). We chose $\sigma_1 = 1$ (conductivity of the lungs during expiration), $\sigma_2 = 2.8$ (conductivity of the liver) and $\sigma_3 = 6.7$ (conductivity of the blood). We assumed that $L = 32$, i.e., and that current was injected to Ω at 32 locations of the electrodes e_l.

Table 1. Conductivities of healthy tissues

Tissue	Conductivity (mS/cm)
Cerebrospinal fluid (C.S.F)	15.4
Blood	6.7
Liver	2.8
Skeletal muscle (longitudinal)	8
Skeletal muscle (transverse)	0.6
Cardiac muscle (longitudinal)	6.3
Cardiac muscle (transverse)	2.3
Neural tissue	1.7
Grey matter	3.5
White matter	1.5
Lung (expiration)	1
Lung (inspiration)	0.4
Fat	0.36
Bone	0.06

We solved the partial differential equation (1) with boundary conditions (3)-(5) using the FEM. The two-dimensional domain Ω was decomposed into elements Ω_k, and in each element the unknown potential was represented by a linear function. Where the elements intersect, they are required to intersect only in whole edges or at vertices, and the potential is assumed continuous across edges. The FEM generally converges to the (weak) solution of the partial differential equation as the elements become more numerous.

Meshing was performed to discretize the geometry created into elements using a set of grids or nodes. Triangulation was found to be a flexible and well-established way to create meshes with triangular elements. Taking into account that σ is different for Ω_a and Ω_b and that the L = 32 electrodes were positioned at the boundary, one possible triangulation of Ω is shown in Figure 1.a.

Generally, the boundaries of Ω_a and Ω_b do not coincide with the grid. Thus, we retained the triangulation in Figure 1.a and added few elements at the boundary of Ω_a and Ω_b. Figure 1.b shows the triangulation at the boundaries of Ω_a and Ω_b.

When creating a mesh, each node must be properly numbered. If we have a mesh with a 35 x 35 grid then we have at least 1225 nodes and 2312 elements. This is because the nodes and elements at the boundary of the interior cavities are not yet included. One way to number the nodes and elements of the mesh is to retain the numbering of the first mesh (Figure 1.1) and just add the nodes and elements created by the boundaries of Ω_a and Ω_b (Figure 1.2). This means that the locations of the interior cavities can be arbitrary.

We now present the variational formulation of (1). We take any $v \in H^1(\Omega)$, multiply this to (1) and integrate over Ω,

$$\int_{\Omega} -v\nabla \cdot (\sigma \nabla \phi)\, dA = 0. \tag{8}$$

Applying Green's theorem and the Divergence theorem, we get,

$$\int_{\Omega} \sigma \nabla \phi \cdot \nabla v\, dA = \int_{\partial\Omega} \sigma \nabla \phi \cdot \mathrm{n}\, v dS. \tag{9}$$

In view of the boundary condition in (4), we further have,

$$\int_{\Omega} \sigma \nabla \phi \cdot \nabla v\, dA = \int_{\partial\Omega} \sigma \nabla \phi \cdot \mathrm{n}\, v dS = \int_{\Gamma} \sigma \nabla \phi \cdot \mathrm{n}\, v dS. \tag{10}$$

Assuming that $z_l \neq 0$ on e_b we may write (5) as,

$$\sigma \nabla \phi \cdot \mathrm{n} = \frac{1}{z_l}(V_l - \phi). \tag{11}$$

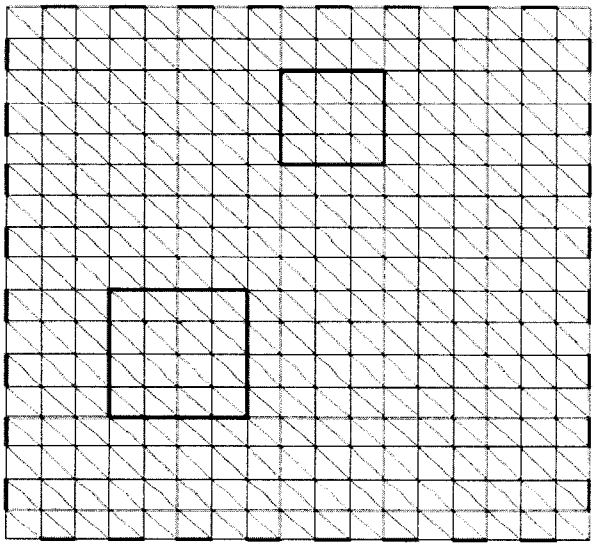

Figure 1.a. A triangulation of the body Ω with cavities Ω_a and Ω_b

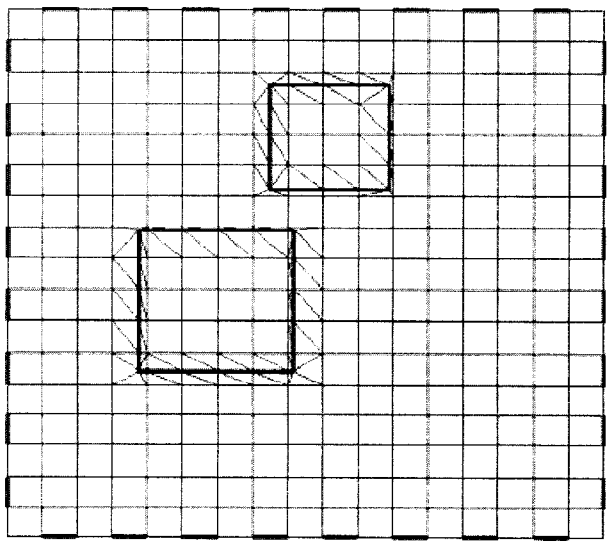

Figure 1.b. A triangulation at the boundaries of Ω_a and Ω_b

So (10) becomes,

$$\int_\Omega \sigma\nabla\phi\cdot\nabla v\,dA+\sum_{l=1}^{L}\int_{e_l}\frac{1}{z_l}\phi v dS-\sum_{l=1}^{L}\int_{e_l}\frac{1}{z_l}V_l v dS=0. \tag{12}$$

This is the variational formulation of (1). The goal is to find $\phi\in H^1(\Omega)$ such that (12) holds for all $v\in H^1(\Omega)$. In our approximation, we will use the conforming Galerkin approach. That is, we will find a solution ϕ in a finite-dimensional closed subspace V_h of $H^1(\Omega)$ such that (12) holds for all $v\in V_h$. We can choose V_h to be the span of the basis $\{w_i\}_{i=1}^N$ that would approximate the potential ϕ. A natural basis is the linear function with value 1 on the ith node and 0 on the other nodes. With this, ϕ can be approximated by,

$$\phi\approx\sum_{i=1}^{N}\phi_i w_i, \tag{13}$$

where N is the number of nodes. The vector $(\phi_1,\ldots,\phi_N)^T$ is the discrete approximation of the potential ϕ. We approximate v using the same $\{w_i\}_{i=1}^N$, i.e., let $v=\sum_{i=1}^{N}v_i w_i$. Together with (12) and (13), we obtain,

$$\sum_{i=1}^{N}\left\{\int_\Omega \sigma\nabla w_i\cdot\nabla w_j\,dA+\sum_{l=1}^{L}\int_{e_l}\frac{1}{z_l}w_i w_j dS\right\}-\sum_{l=1}^{L}\left\{\int_{e_l}\frac{1}{z_l}w_j dS\right\}V_l=0 \tag{14}$$

With known total current on each electrode and the assumption that z_l is constant on e_l, we can combine (3) and (5) to get,

$$\begin{aligned} I_l &= \int_{e_l}\frac{1}{z_l}(V_l-\phi)dS \\ &= \frac{1}{z_l}|e_l|V_l-\sum_{j=1}^{N}\left\{\int_{e_l}\frac{1}{z_l}w_j dS\right\}\phi_j, \end{aligned} \tag{15}$$

where $|e_l|$ is the length of the lth electrode.

Equations (14) and (15) yield the linear system,

$$\begin{bmatrix} M+Z & W \\ W^T & D \end{bmatrix}\begin{bmatrix}\phi\\ V\end{bmatrix}=\begin{bmatrix}0\\ I\end{bmatrix}, \tag{16}$$

where $D=\mathrm{diag}(|e_l|/z_l)$ and the other matrices have components given by,

$$\begin{aligned} M_{ij} &= \int_\Omega \sigma\nabla w_i\cdot\nabla w_j\,dA, \\ Z_{ij} &= \sum_{l=1}^{L}\int_{e_l}\frac{1}{z_l}w_i w_j dS \quad \text{and} \\ W_{lj} &= -\int_{e_l}\frac{1}{z_l}w_j dS. \end{aligned} \tag{17}$$

Since σ is piecewise constant and because of the way we triangulated Ω, σ is constant in each element. This is advantageous because σ can be taken out of the integral over each element k. Moreover, the quantity $\nabla w_i\cdot\nabla w_j$ is constant because our basic functions are linear. These considerations imply that,

$$\int_\Omega \sigma\nabla w_i\cdot\nabla w_j\,dA=\sum_{k=1}^{K}\sigma_k\int_{\Omega_k}\nabla w_i\cdot\nabla w_j\,dA=\sum_{k=1}^{K}\sigma_k\,(\nabla w_i\cdot\nabla w_j)|\Omega_k|, \tag{18}$$

where K is the number of elements and σ_k is the conductivity on Ω_k. Observe that the quantity $(\nabla w_i\cdot\nabla w_j)|\Omega_k|$ depends on the mesh but not on σ, so it can be precalculated. This observation would save us a considerable amount of computation time.

Because z_l can be any positive constant value we chose it to be 3. We chose the value of I_l to be either 1 or -1. By doing this (6) is satisfied.

If we have N nodes and L electrodes, then the matrix of the linear system (18) has dimensions $(N+L)\times(N+L)$, and is sparse because the nonzero row entries of the matrix M depend only on the neighbouring vertices connected to any given vertex by an edge. Because of this sparseness, the system (18) was solved by LU factorization. We used the lusolve command in Scilab.

Solving the inverse problem

The inverse EIT problem, also known as image reconstruction, is the recovery of the coefficient σ in the elliptic PDE (1) given the boundary data I_l and V_l on each electrode. Since it is logical to assume that a body has a unique conductivity distribution, the solution to the inverse EIT problem exists. However, it is known that the EIT problem is severely ill-posed, that is, small changes in the boundary voltages give arbitrary large changes in the conductivity distribution.

The methods used for solving the reconstruction problem search for an approximate conductivity distribution by minimizing some sort of residual involving the measured and calculated boundary voltages. We define the operator F by $F(x,\sigma) = V$ which gives the boundary voltages V of any arbitrary conductivity distribution σ with geometry x (that is, locations of the subregions Ω_a and Ω_b inside Ω). V is computed by solving (16).

In this study, we used evolutionary optimization methods to solve the reconstruction problem. We iteratively reconstructed an image that fits best the measured voltage V_l^m at the lth electrode. At each iteration, we calculated the voltages at each electrode $F_l(x,\sigma) = V_l$ that correspond to the present state of the reconstructed image. By minimizing the relative error between the measured and the calculated voltages, we expected the reconstructed image to converge with the original image. In other words, we minimized the cost function,

$$C(x,\sigma) = \sum_{i=1}^{L} \left(\frac{V_i^m - F_i(x,\sigma)}{V_i^m} \right)^2 . \qquad (19)$$

This minimization problem is now an unconstrained problem in several variables. We can treat this problem differently:

- We can assume that the geometry is known. This means that we only have to solve for the conductivities σ_1, σ_2 and σ_3 at Ω_a, Ω_b and $\Omega \backslash (\Omega_a \cup \Omega_b)$, respectively. Therefore (19) is now an unconstrained optimization problem in 3 variables.
- We can assume that the conductivities σ_1, σ_2 and σ_3 are known. We then try to locate the Ω_a and Ω_b. Because these regions are both squares, to locate them, we can simply find their centers (h_1, k_1) and (h_2, k_2), and their dimension $2s_1$ and $2s_2$. Hence (19) is now an optimization problem in 6 variables.
- We can assume that both geometry and the conductivities are unknown. Thus, we have to solve the optimization problem in 9 variables.

To minimize (19), we used the Genetic Algorithm hybridized with the following optimization methods: the Nelder-Mead Downhill Simplex method, a Quasi-Newton method, and the Simulated Annealing method. We briefly discuss below the implementations of these methods.

The Genetic Algorithm (GA) is a probabilistic method based on Darwin's Theory of Evolution. An initial population is generated and this population is transformed into a "better" population per iteration. This transformation consists of processes that resemble biological phenomena such as natural selection, reproduction, and mutation. GA starts with an initial population. For example, if we are optimizing a cost functional of 3 variables, the initial population consists of vectors of size 3. The members of the population serve as our initial guesses. The number of population is usually 8 to 9 times the number of variables. A natural selection is performed by finding the individuals with low function values. A percentage of the population (selection rate) is then rejected based on the value of their cost functional. Naturally, those members with high cost function values are rejected. Reproduction is implemented next. This involves randomly selecting two parents from the mating pool, which is the set of all members who survived the selection process. These two are then used to create new offspring. The next step is mutation. This means that a percentage of the new population will be replaced by random individuals. This will ensure that the method will not get stuck in a local minimum. We also perform elitism: a method by which the best individual in the current generation cannot be replaced by mutation. This new pool of individuals will comprise the new generation and the process is repeated.

One advantage of the GA is that it approximates not just a minimum but a global minimum. Although convergence properties of the GA are not mathematically established, it has shown good performance in practice. In our implementation of GA, we used the following parameters: 0.5 for the selection rate and 0.1 for the mutation rate. Moreover, we used Michalewicz's non-uniform mutation, i.e., a member p_i of the population randomly mutates into either $p_i + \delta(\max(pop) - pi)$ or $p_i - \delta(p_i - \min(pop))$ where pop is the current population, $\delta = \gamma(1 - gen/maxgen)^B$, γ is a random number in (0, 1) and B is the weight exponent, which can range from 1.0 to 5.0 but we set equal to 2.0. This type of mutation is mentioned in Cormier and Boudreau (2001) and da Silva Barra and others (2006). To deal with the ill-posedness, we limit our search space to $\pm 20\%$ of the true value of the desired quantities.

One problem with GA is that it needs a lot of function evaluations. For instance, for a population of 50 and a number of generations of 100, 5000 function evaluations are needed. This study will involve as few evaluations as possible to cut down on computation time. This is the where the local minimizers will be helpful. The Nelder-Mead Downhill Simplex method, a Quasi-Newton method and the Simulated Annealing method will do the rest of the optimization. The role of GA is to put the estimate in the right valley and the local minimizers will reach the minimum with better accuracy and speed.

Nelder and Mead's Downhill Simplex method is a simple iterative, multidimensional minimization method. It does not require the existence of the derivative and instead uses function evaluations to obtain the minimum. At the beginning of each iteration, $n + 1$ linearly independent points labelled x_1, x_2, ..., x_{n+1} are considered. These points are ordered so that $f(x_{n+1}) \geq f(x_n) \geq \cdots \geq f(x_1)$. These points will serve as vertices of an n-dimensional convex volume called a simplex. The method will then attempt to enclose the minimum inside the simplex. Each iteration produces a new point that will replace x_{n+1}, the point where the function value is highest, thus creating a new simplex. The algorithm stops if either of the following criteria is satisfied: (a) $\sum_{i=2}^{n+1} |f(x_i) - f(x_1)| < \epsilon$ or (b) $\sum_{i=2}^{n+1} \|x_i - x_1\| < \epsilon$ for some tolerance ϵ. The first criterion is used to check if the function value has decreased enough while the second criterion is used to check if the current simplex is small enough.

Although the inverse EIT problem is severely ill-posed, the cost function is still smooth, hence we can attempt a gradient-based algorithm. One problem with this approach is that near the minimum, the cost function is almost flat. However, with a good starting point this method could prove effective. Different gradient-based algorithms are available but in this work, we limit ourselves to a method that only uses the first derivative information of the cost function. One such method is a Quasi-Newton method that uses the BFGS updating formula, named after its developers Broyden, Fletcher, Goldfarb, and Shann. This method will be subsequently referred to as the BFGS Quasi-Newton method. In this method we use estimate $x_k = x_{k-1} + \alpha_{k-1} p_{k-1}$ where α_{k-1} is the step length and p_{k-1} is an approximation of the Hessian using only the first derivative. We terminate this method when either: (a) $\|x_k - x_{k-1}\| < \epsilon$ or (b) $|f(x_k) - f(x)| < \epsilon$ where ϵ is the tolerance.

Simulated Annealing (SA) is a probabilistic method proposed by Kirkpatrick and co-workers that mimics the annealing process: a substance is heated above its melting temperature and then gradually cooled to produce the crystalline lattice that minimizes its energy probability distribution. Suppose our estimate of the minimum is x_{k-1} and let $x_k = x_{k-1} + \Delta x$ be the new estimate obtained from the old. In most minimization methods, if $f(x_k) > f(x_{k-1})$, then x_k is rejected, but in SA it is accepted with a probability of $\exp\left(-\frac{f(x_k) - f(x_{k-1})}{T_k}\right)$ where T_k decreases as k becomes large. This allows SA to reach an approximation to the global minimum. SA is terminated when either: (a) $\|x_k - x_{k-1}\| < \epsilon$ or (b) $|T_k| < \epsilon$ where ϵ is the tolerance.

Because the minimum lies in a flat valley, we chose the tolerance ϵ to be of order 10^{-14}. Detailed discussions of all the above methods may be found in Haupt and Haupt (2004), Fletcher (1980), or in other texts on optimization.

Since the study uses Hybrid GA, the need to find an accurate solution upon its implementation is eliminated. Also, this study would like to keep the number of generations to be as small as possible. To determine how many generations will be used, the researchers checked the function value and the change in function value at the best individual of the population. Figure 2 shows the convergence of GA for the case when the conductivity values are given and the geometry of Ω is known. Note that after 50 generations, the function values of the best individuals did not change much, a signal to terminate GA. This was also observed after several more runs. So we decided to let GA run for only 50 generations. Likewise, by observing the convergence of GA in the case when the geometry of Ω is given and σ is unknown, we terminated GA after 20 generations. Finally, in the case when both the geometry and the conductivity distribution of Ω are unknown, we terminated GA after 100 generations.

Because we intended to compare different hybrids of the GA, we deemed it reasonable to store the results obtained from the GA and use the same starting point for all the local optimizers. When shifting from the GA to the Nelder-Mead method, we used the best member of the GA population to generate the initial simplex that consisted of $n + 1$ points. Moving from the GA to either the BFGS Quasi-Newton method or the SA method was not a problem because both methods only needed one starting point.

We note that while we used the standard way of implementing the Nelder-Mead and BFGS Quasi-Newton methods, we used a different updating formula in our implementation of the SA. The usual update is simply $x_k + \beta u$, where u is a random unit vector in $[-1, 1]$ and β is a constant vector which defines the maximum change allowed in each variable. Instead of this, we used the update $x_k + \beta u(1 - k/\max\{k\})$, an original innovation based on the observation that as the number of iterations reaches the maximum allowed, the change in x_k will be minimal. In other words, we do not want the next iterate to go too far away from the current approximate solution.

All numerical simulations were implemented in Scilab, an open-source program for numerical computations freely downloadable online.

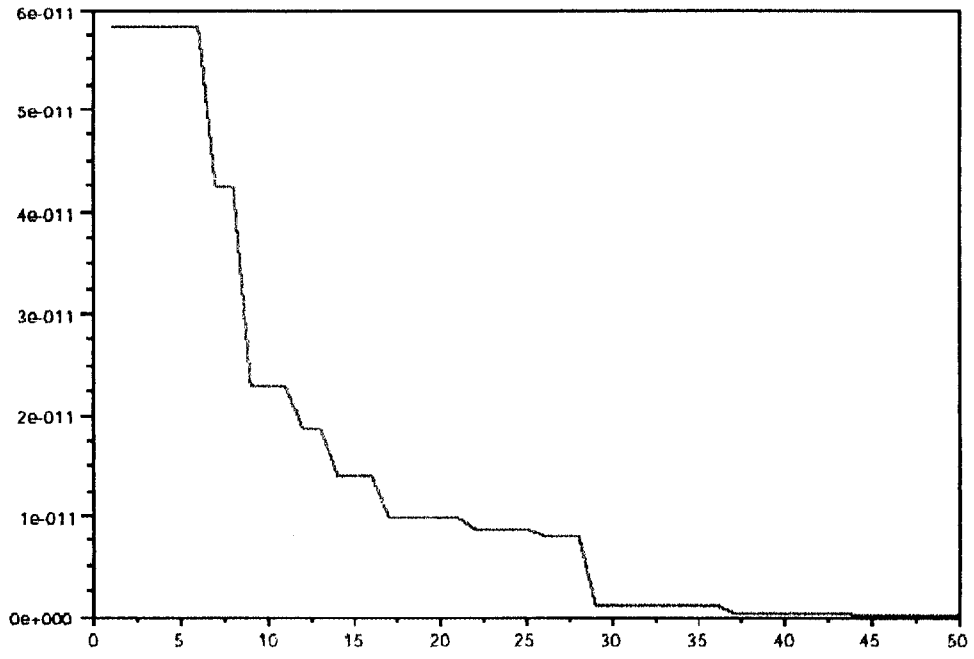

Figure 2. Convergence plot of the GA for the case when σ is given but the geometry is unknown

NUMERICAL RESULTS

As discussed in the previous section, the following cases were studied:

1) recovery of the conductivities when the geometry of Ω is given;
2) reconstruction of the geometry of Ω when conductivity values are known; and
3) simultaneous recovery of the conductivity distribution and geometry reconstruction of Ω.

In all these cases, we used hybrids of the GA. We implemented the GA first and then used different local minimizers to finish the rest of the optimization. We compared the performances of three hybrids of GA first with the Nelder-Mead method, then with the BFGS Quasi-Newton method, and finally with the Simulated Annealing. In each of these three cases, we performed ten (10) runs for each hybrid of GA.

Recovery of the conductivities

Here the exact location of Ω_a and Ω_b are both given. The goal now is to find the conductivities inside these cavities and the conductivity outside them. Let the conductivities of Ω_a , Ω_b and $\Omega \setminus (\Omega_a \cup \Omega_b)$ be σ_1, σ_2 and σ_3, respectively. The actual values used are $\sigma_1 = 1.0$, $\sigma_2 = 2.8$ and $\sigma_3 = 6.7$. The recovered conductivities by the three hybrids of GA are shown in Tables 2, 3 and 4.

On average, the hybrid of the GA with the SA obtained the best results. Of all thirty runs, the best result was also obtained by the GA-SA hybrid with cost equal to 1.660×10^{-14} , and with $\sigma_1 = 1.002$, $\sigma_2 = 2.799$ and $\sigma_3 = 6.700$. Without the use of the SA, the values of the conductivities estimated by GA alone were $\sigma_1 = 1.040$, $\sigma_2 = 2.749$ and $\sigma_3 = 6.693$. Although the cost functional of these values is 2.641×10^{-12}, we can see that using a hybrid of the GA with the SA gave a more precise approximation. The approximated conductivities are within 1% of the actual values.

Table 2. Recovered conductivities using GA with Nelder-Mead method when the geometry is known

Run	σ_1	σ_2	σ_3	Cost
1	1.002	2.798	6.700	1.672×10^{-14}
2	1.008	2.780	6.700	3.415×10^{-14}
3	1.037	2.738	6.698	30.10×10^{-14}
4	0.979	2.858	6.700	18.91×10^{-14}
5	0.978	2.857	6.700	18.60×10^{-14}
6	1.022	2.822	6.697	22.98×10^{-14}
7	1.002	2.799	6.700	1.661×10^{-14}
8	0.980	2.839	6.701	12.88×10^{-14}
9	0.997	2.810	6.700	2.355×10^{-14}
10	**1.001**	**2.800**	**6.700**	$\mathbf{1.658 \times 10^{-14}}$
Mean	1.001	2.810	6.700	11.42×10^{-14}

The run with the least cost is in boldfaced characters.

Table 3. Recovered conductivities using GA with the BFGS Quasi-Newton method when the geometry is known

Run	σ_1	σ_2	σ_3	Cost
1	1.000	2.803	6.700	1.743×10^{-14}
2	1.009	2.778	6.700	3.830×10^{-14}
3	1.025	2.734	6.699	22.16×10^{-14}
4	0.980	2.859	6.700	18.68×10^{-14}
5	0.998	2.808	6.700	1.991×10^{-14}
6	1.005	2.790	6.700	2.058×10^{-14}
7	1.002	2.798	6.700	1.661×10^{-14}
8	1.001	2.799	6.700	1.662×10^{-14}
9	1.000	2.801	6.700	1.678×10^{-14}
10	**1.001**	**2.799**	**6.700**	$\mathbf{1.657 \times 10^{-14}}$
Mean	1.002	2.797	6.700	5.712×10^{-14}

The run with the least cost is in boldfaced characters.

Table 4. Recovered conductivities using GA with SA when the geometry is known

Run	σ_1	σ_2	σ_3	Cost
1	1.002	2.796	6.700	1.720×10^{-14}
2	1.004	2.800	6.700	1.844×10^{-14}
3	1.004	2.791	6.700	1.951×10^{-14}
4	1.001	2.798	6.700	1.686×10^{-14}
5	1.002	2.802	6.700	1.808×10^{-14}
6	1.002	2.803	6.700	1.835×10^{-14}
7	**1.002**	**2.799**	**6.700**	$\mathbf{1.660 \times 10^{-14}}$
8	1.003	2.795	6.700	1.753×10^{-14}
9	1.002	2.796	6.700	1.710×10^{-14}
10	1.001	2.799	6.700	1.679×10^{-14}
Mean	1.002	2.798	6.700	1.765×10^{-14}

The run with the least cost is in boldfaced characters.

Geometry reconstruction

Suppose that the locations of Ω_a and Ω_b are both unknown but the conductivities are known as σ_1, σ_2 and σ_3. Let (h_1, k_1) and (h_2, k_2) be the centers of the squares Ω_a and Ω_b with sides of length $2s_1$ and $2s_2$, respectively. The actual values are $(h_1, k_1) = (0.35, 0.45)$, $(h_2, k_2) = (0.54, 0.76)$, $s_1 = 0.13$ and $s_2 = 0.1$.

The reconstructed geometry by the three hybrids of GA are shown in Tables 5, 6 and 7. On average, the hybrid of the GA with the SA obtained the best results. As in the previous case, the best result among the thirty runs was also obtained by the GA-SA hybrid with cost 1.542×10^{-14} and with $(h_1, k_1) = (0.350, 0.450)$, $s_1 = 0.130$, $(h_2, k_2) = (0.540, 0.760)$ and $s_2 = 0.100$. These are within 1% of the actual value, which is better compared to the results obtained by da Silva Barra and

others (2006), in which the best residual they obtained was 14.8%. Moreover, the result from the hybrid of the GA and the SA is a considerable improvement compared to the result when the GA is implemented alone. Without the SA, the approximated solutions are: $(h_1, k_1) = (0.361, 0.465)$, $s_1 = 0.136$, $(h_2, k_2) = (0.520, 0.824)$ and $s_2 = 0.087$. The obtained geometries by the three hybrid methods are illustrated in Figures 3 and 4.

Table 5. Reconstructed geometry using Hybrid GA with the Nelder-Mead method when conductivity values are known

Run	(h_1, k_1)	(h_2, k_2)	s_1	s_2	Cost
1	**(0.351, 0.451)**	**(0.538, 0.766)**	**0.131**	**0.098**	$\mathbf{5.967 \times 10^{-14}}$
2	(0.347, 0.449)	(0.535, 0.763)	0.129	0.102	18.50×10^{-14}
3	(0.363, 0.459)	(0.528, 0.800)	0.135	0.088	144.7×10^{-14}
4	(0.352, 0.448)	(0.545, 0.747)	0.129	0.102	18.12×10^{-14}
5	(0.347, 0.448)	(0.539, 0.755)	0.129	0.102	6.829×10^{-14}
6	(0.356, 0.443)	(0.554, 0.743)	0.129	0.101	120.7×10^{-14}
7	(0.352, 0.453)	(0.545, 0.757)	0.131	0.099	28.88×10^{-14}
8	(0.341, 0.441)	(0.545, 0.735)	0.126	0.109	99.67×10^{-14}
9	(0.354, 0.451)	(0.544, 0.759)	0.131	0.098	15.07×10^{-14}
10	(0.353, 0.452)	(0.542, 0.763)	0.131	0.097	16.96×10^{-14}
Mean	(0.352, 0.450)	(0.542, 0.759)	0.130	0.100	47.54×10^{-14}

The run with the least cost is in boldfaced characters.

Table 6. Reconstructed geometry using Hybrid GA with the BFGS Quasi-Newton method when conductivity values are known

Run	(h_1, k_1)	(h_2, k_2)	s_1	s_2	Cost
1	(0.353, 0.455)	(0.535, 0.767)	0.132	0.098	22.38×10^{-14}
2	(0.346, 0.450)	(0.533, 0.767)	0.130	0.101	21.75×10^{-14}
3	(0.359, 0.463)	(0.521, 0.824)	0.136	0.088	247.1×10^{-14}
4	(0.355, 0.446)	(0.551, 0.737)	0.129	0.102	71.59×10^{-14}
5	(0.346, 0.449)	(0.540, 0.756)	0.129	0.103	11.50×10^{-14}
6	(0.359, 0.444)	(0.557, 0.725)	0.129	0.103	192.6×10^{-14}
7	(0.352, 0.452)	(0.542, 0.760)	0.131	0.099	7.979×10^{-14}
8	(0.347, 0.439)	(0.548, 0.726)	0.126	0.109	119.4×10^{-14}
9	(0.352, 0.449)	(0.544, 0.767)	0.131	0.097	36.19×10^{-14}
10	**(0.350, 0.450)**	**(0.538, 0.765)**	**0.130**	**0.099**	$\mathbf{5.015 \times 10^{-14}}$
Mean	(0.352,0.450)	(0.541, 0.759)	0.130	0.100	10.81×10^{-14}

The run with the least cost is in boldfaced characters.

Table 7. Reconstructed geometry using Hybrid GA with the Simulated Annealing method when conductivity values are known

Run	(h_1, k_1)	(h_2, k_2)	s_1	s_2	Cost
1	(0.351, 0.452)	(0.539, 0.765)	0.131	0.098	4.559×10^{-14}
2	(0.349, 0.449)	(0.540, 0.758)	0.130	0.101	1.655×10^{-14}
3	(0.352, 0.453)	(0.538, 0.769)	0.131	0.097	9.552×10^{-14}
4	(0.350, 0.450)	(0.540, 0.760)	0.130	0.100	1.657×10^{-14}
5	(0.349, 0.449)	(0.540, 0.756)	0.129	0.101	2.542×10^{-14}
6	(0.349, 0.449)	(0.541, 0.756)	0.130	0.101	2.182×10^{-14}
7	**(0.350, 0.450)**	**(0.540, 0.760)**	**0.130**	**0.100**	$\mathbf{1.542 \times 10^{-14}}$
8	(0.348, 0.448)	(0.541, 0.753)	0.129	0.102	5.944×10^{-14}
9	(0.351, 0.451)	(0.539, 0.762)	0.130	0.099	2.479×10^{-14}
10	(0.351, 0.452)	(0.538, 0.766)	0.131	0.098	5.941×10^{-14}
Mean	(0.350,0.450)	(0.540, 0.761)	0.130	0.100	3.805×10^{-14}

The run with the least cost is in boldfaced characters.

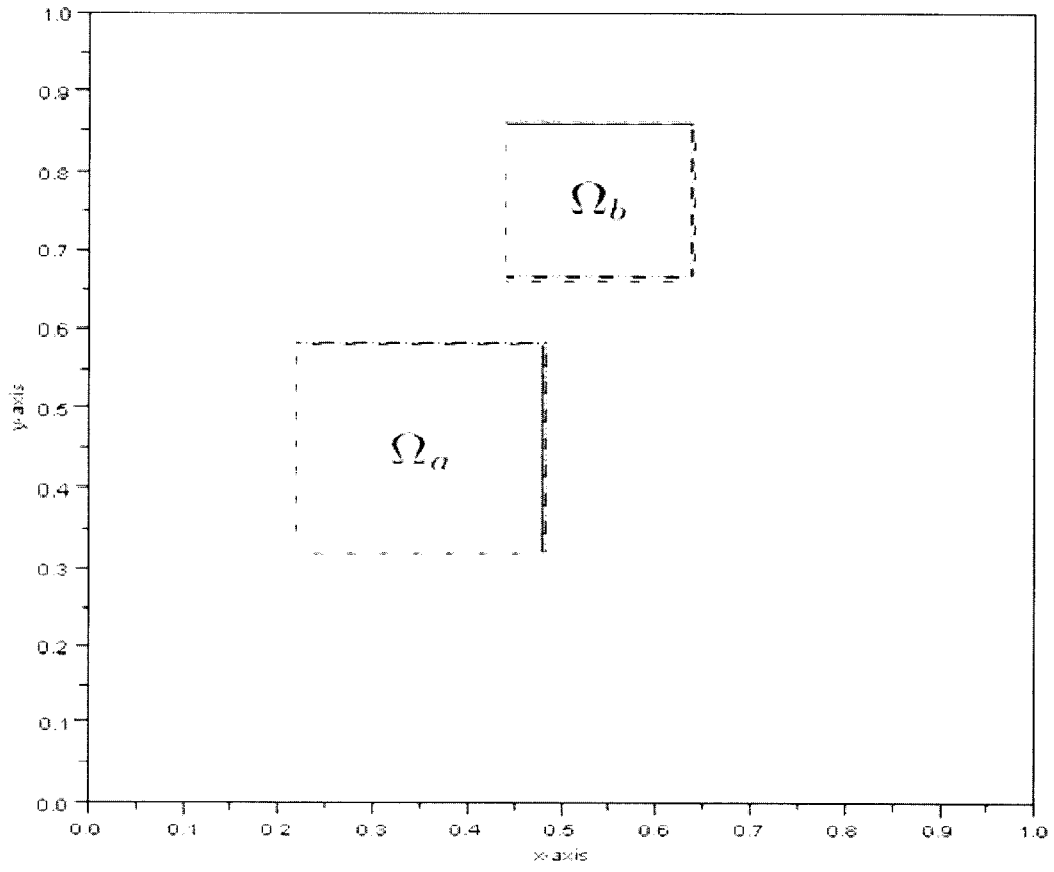

Figure 3. The obtained geometry of Ω, when the conductivities are known, by the hybrid of GA with the Nelder-Mead method (blue dotted line), with the BFGS Quasi-Newton method (red dash-dotted line) and the SA method (green dashed line). The actual geometry of Ω is the black square (covered by the other colored squares).

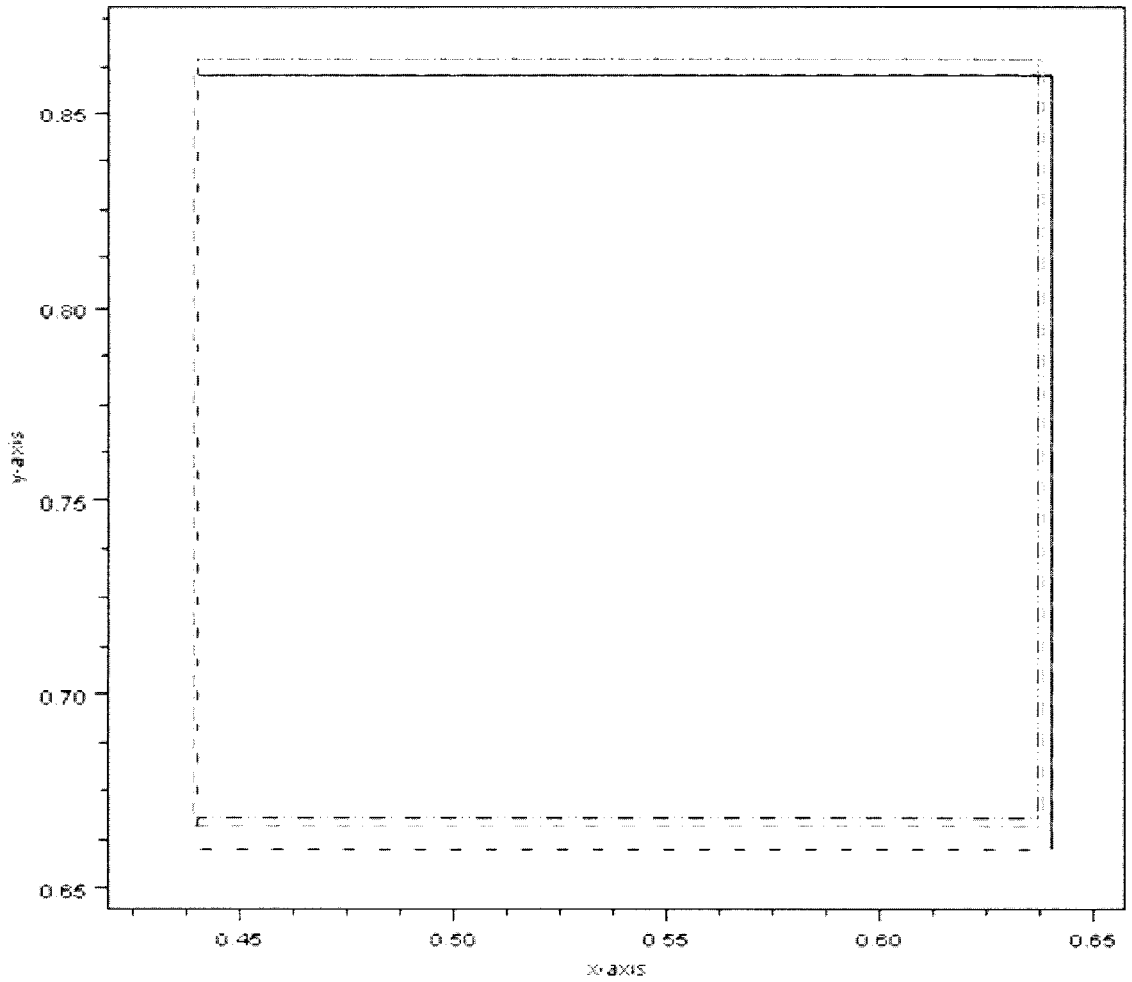

Figure 4. A magnified portion of Figure 3 showing the geometry of Ω_b

Simultaneous recovery of conductivities and geometry reconstruction

Finally, we tried to simultaneously recover the conductivities and reconstruct the geometry of Ω using the three methods. This means that the location of Ω_a and Ω_b and the conductivities are both unknown. The obtained results are shown in Tables 8, 9 and 10. On average, the hybrid of the GA with the SA obtained the best results. Of all the thirty runs, the best result was also obtained by the GA-SA hybrid with cost 5.395×10^{-14}, and with $(h_1, k_1) = (0.350, 0.446)$, $(h_2, k_2) = (0.542, 0.752)$, $s_1 = 0.126$, $s_2 = 0.100$, $\sigma_1 = 0.846$, $\sigma_2 = 2.694$ and $\sigma_3 = 6.702$. The obtained geometries are illustrated in Figures 5 and 6. Note that while the centers and dimensions of the square cavities are within 3% of the actual values, the conductivities are off the mark by about 7%. Still, a significant improvement can be observed from the result obtained by using the GA alone; $(h_1, k_1) = (0.368, 0.464)$, $(h_2 k_2) = (0.556, 0.747)$, $s_1 = 0.136$, $s_2 = 0.95$, $\sigma_1 = 1.123$, $\sigma_2 = 2.923$ and $\sigma_3 = 6.692$. The best results obtained by the other two methods are not far away from the best result of the GA-SA hybrid. The cost in the GA-Nelder Mead hybrid is 6.083×10^{-13} while that in the GA-BFGS Quasi-Newton hybrid is 4.030×10^{-13}.

Table 8. Reconstructed geometry and recovered conductivity distribution using Hybrid GA with the Nelder-Mead method

Run	(h_1, k_1)	(h_2, k_2)	s_1	s_2	σ_1	σ_2	σ_3	Cost
1	(0.368, 0.464)	(0.556, 0.746)	0.137	0.095	1.123	2.922	6.694	33.60×10^{-13}
2	(0.368, 0.462)	(0.534, 0.773)	0.138	0.088	1.115	2.758	6.705	35.06×10^{-13}
3	(0.351, 0.441)	(0.545, 0.724)	0.126	0.098	0.952	2.284	6.701	21.75×10^{-13}
4	(0.376, 0.456)	(0.555, 0.754)	0.133	0.096	0.898	3.045	6.707	56.73×10^{-13}
5	(0.351, 0.445)	(0.551, 0.725)	0.128	0.108	0.983	2.904	6.703	12.51×10^{-13}
6	(0.331, 0.430)	(0.533, 0.722)	0.124	0.111	1.104	2.403	6.714	28.34×10^{-13}
7	**(0.353, 0.447)**	**(0.536, 0.769)**	**0.132**	**0.103**	**1.05**	**3.143**	**6.701**	$\mathbf{6.083 \times 10^{-13}}$
8	(0.371, 0.451)	(0.556, 0.730)	0.133	0.096	1.045	2.774	6.701	42.55×10^{-13}
9	(0.360, 0.448)	(0.545, 0.730)	0.127	0.101	0.824	2.694	6.703	15.99×10^{-13}
10	(0.359, 0.467)	(0.542, 0.792)	0.131	0.088	0.895	2.843	6.683	21.68×10^{-13}
Mean	(0.359, 0.451)	(0.545, 0.746)	0.131	0.098	0.999	2.777	6.701	27.42×10^{-13}

The run with the least cost is in boldfaced characters.

Table 9. Reconstructed geometry and recovered conductivity distribution using Hybrid GA with the BFGS Quasi-Newton method

Run	(h_1, k_1)	(h_2, k_2)	s_1	s_2	σ_1	σ_2	σ_3	Cost
1	(0.368, 0.464)	(0.556, 0.747)	0.136	0.095	1.123	2.923	6.693	33.84×10^{-13}
2	(0.366, 0.463)	(0.541, 0.781)	0.137	0.087	1.104	2.785	6.697	15.73×10^{-13}
3	(0.347, 0.432)	(0.534, 0.732)	0.126	0.102	0.953	2.304	6.718	25.07×10^{-13}
4	(0.368, 0.449)	(0.549, 0.747)	0.130	0.100	0.890	3.038	6.695	27.03×10^{-13}
5	**(0.351, 0.442)**	**(0.543, 0.744)**	**0.128**	**0.106**	**0.991**	**2.937**	**6.706**	$\mathbf{4.030 \times 10^{-13}}$
6	(0.340, 0.438)	(0.534, 0.721)	0.128	0.108	1.105	2.405	6.718	15.99×10^{-13}
7	(0.355, 0.448)	(0.536, 0.769)	0.132	0.103	1.050	3.143	6.701	4.759×10^{-13}
8	(0.361, 0.439)	(0.560, 0.737)	0.131	0.100	1.066	2.800	6.700	26.28×10^{-13}
9	(0.350, 0.441)	(0.547, 0.735)	0.124	0.104	0.826	2.695	6.705	4.269×10^{-13}
10	(0.356, 0.465)	(0.545, 0.793)	0.131	0.089	0.895	2.804	6.682	19.26×10^{-13}
Mean	(0.356, 0.446)	(0.544, 0.746)	0.130	0.100	1.012	2.781	6.704	24.47×10^{-13}

The run with the least cost is in boldfaced characters.

Table 10. Reconstructed geometry and recovered conductivity distribution using Hybrid GA with the Simulated Annealing method

Run	(h_1, k_1)	(h_2, k_2)	s_1	s_2	σ_1	σ_2	σ_3	Cost
1	(0.353, 0.454)	(0.539, 0.767)	0.133	0.099	1.049	2.897	6.699	8.843×10^{-14}
2	(0.360, 0.459)	(0.540, 0.787)	0.135	0.090	1.085	2.797	6.694	67.79×10^{-14}
3	(0.346, 0.443)	(0.542, 0.740)	0.127	0.099	0.967	2.352	6.705	22.17×10^{-14}
4	(0.356, 0.452)	(0.544, 0.765)	0.130	0.098	0.942	2.942	6.697	30.08×10^{-14}
5	(0.351, 0.447)	(0.543, 0.747)	0.129	0.105	0.991	2.937	6.702	11.59×10^{-14}
6	(0.341, 0.439)	(0.541, 0.726)	0.128	0.108	1.100	2.547	6.709	77.77×10^{-14}
7	(0.352, 0.454)	(0.534, 0.773)	0.133	0.103	1.048	3.140	6.699	10.78×10^{-14}
8	(0.357, 0.452)	(0.544, 0.761)	0.132	0.096	1.044	2.783	6.699	29.25×10^{-14}
9	**(0.350, 0.446)**	**(0.542, 0.752)**	**0.126**	**0.100**	**0.846**	**2.694**	**6.702**	$\mathbf{5.395 \times 10^{-14}}$
10	(0.357, 0.458)	(0.536, 0.787)	0.131	0.092	0.911	2.814	6.694	42.71×10^{-14}
Mean	(0.352, 0.450)	(0.540, 0.760)	0.130	0.099	0.998	2.790	6.700	30.64×10^{-14}

The run with the least cost is in boldfaced characters.

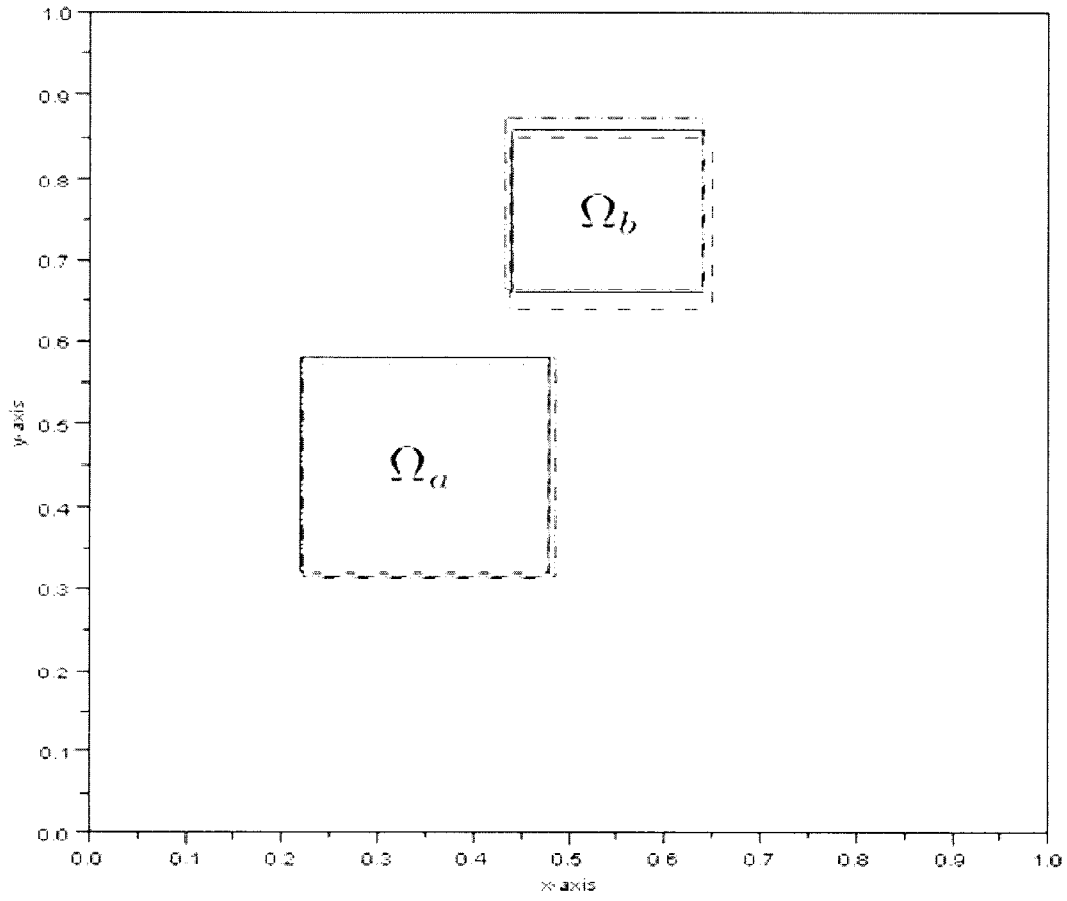

Figure 5. The obtained geometry of Ω when the conductivities are unknown, by the hybrid of GA with the Nelder-Mead method (blue dotted line), with the BFGS Quasi-Newton method (red dash-dotted line) and the SA method (green dashed line). The actual geometry of Ω is the black square (covered by the other colored squares).

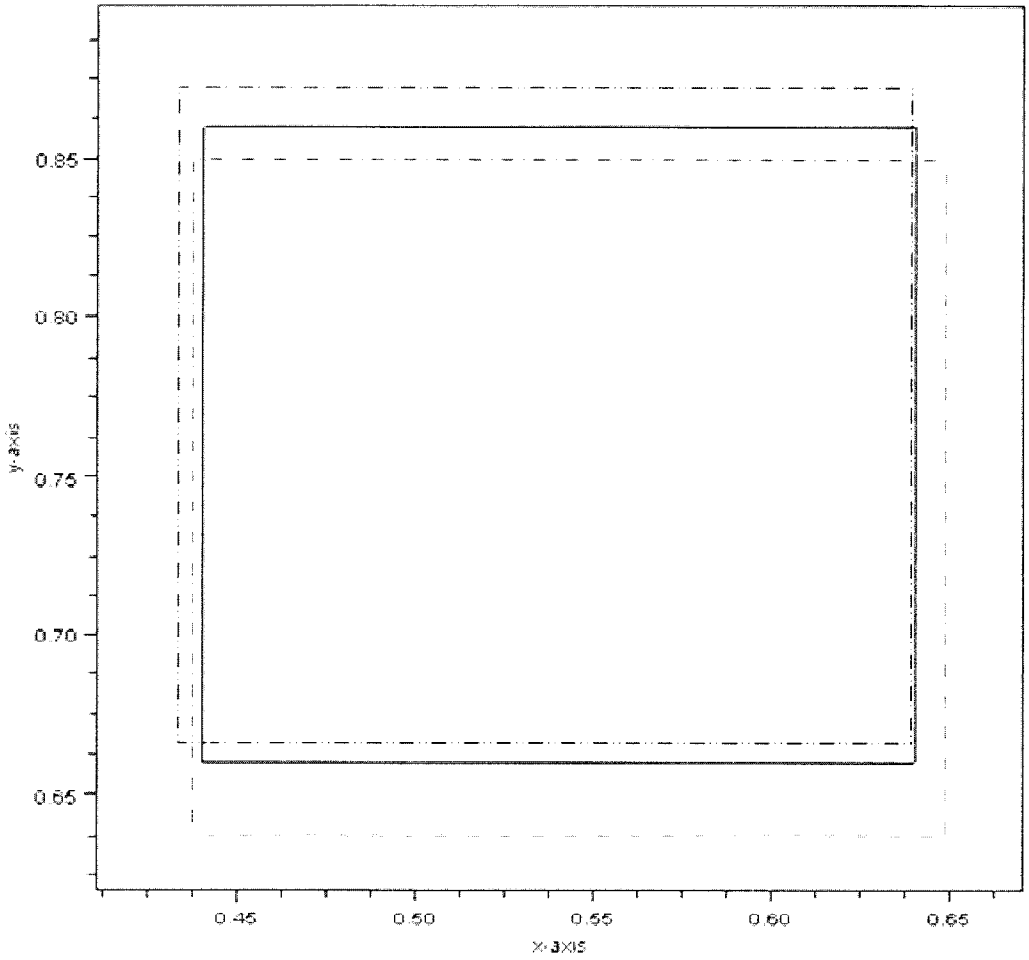

Figure 6. A magnified portion of Figure 5 showing the geometry of Ω_b

CONCLUSIONS

We showed that the hybrids of the GA with Nelder-Mead, the BFGS Quasi-Newton and SA methods could effectively recover the conductivities given the geometry, reconstruct the geometry given the conductivities, or simultaneously perform both. Compared to other optimization methods, GA requires a significant amount of computational time because of the big number of function evaluations done at each generation. However, with the aid of local minimizers, we were able to significantly reduce the number of generations needed, just enough for the GA to give the local optimizers a good initial guess. In our simulations, all three hybrids came up with very low cost function values but generally the GA-SA combination obtained the best results.

This paper considered the case of a square-shaped body with square cavities but it would be desirable to consider a more general geometry in future simulations. This would necessitate the use of a (possibly commercial) finite element method software. The researchers are also looking into the possibility of implementing a regularization procedure to deal with the ill-posedness of the EIT problem.

ACKNOWLEDGMENT

The authors acknowledge the support of the Commission on Higher Education Center of Excellence Research Grant in the conduct of this research.

REFERENCES

Borcea L. 2002. Electrical impedance tomography. Institute of Physics Publishing: Inverse Problems 18: R99-R136.

Cheney M, Isaacson D, Newell J. 1999. Electrical impedance tomography. SIAM Rev 41: 85-101.

Cormier G, Boudreau R. 2001. Real-coded genetic algorithm for Bragg grating parameter synthesis. J Opt Soc Am 18(12): 1771-76.

da Silva Barra LP, Peters F, de Paula Martins C, Barbosa H. 2006. Computational experiments in electrical impedance tomography. Paper presented at the XXVIII CILAMCE; 2006 September 3-6; Belém, Pará, Brazil.

Fletcher R. 1980. Practical methods of optimization volume 1: Unconstrained optimization. NY: John Wiley and Sons. 120 p.

Gray GA. 2002. A variational study of electrical impedance tomography problem [PhD thesis]. Houston, Texas: Rice University. 135 leaves.

Haupt R, Haupt SE. 2004. Practical genetic algorithms. NJ: John Wiley and Sons. 177 p.

Kim H-C, Boo C-J, Lee Y-J. 2005. Image reconstruction using simulated annealing algorithm in EIT. International Journal of Control, Automation, and Systems 3(2): 211-16.

Parker RL. 1984. The inverse problem of resistivity sounding. Geophysics 142: 2143-58.

Santosa F, Kaup P, Vaugelius M. 1996. A method for imaging corrosion damage in thin plates from electrostatic data. Inverse Problem 12: 278-93.

Somersalo E, Cheney M, Isaacson D. 1992. Existence and uniqueness for electrode models of electric current computed tomography. SIAM J Appl Math 52: 1023-40.